Photocatalytic reduction of CO_2 over exposed-crystal-face-controlled TiO_2 nanorod having a brookite phase with co-catalyst loading

Teruhisa Ohno[a,b,c,*], Takayoshi Higo[a], Naoya Murakami[a,c], Hirofumi Saito[a], Qitao Zhang[a], Yin Yang[a], Toshiki Tsubota[a]

[a] Department of Materials Science, Faculty of Engineering, Kyushu Institute of Technology, 1-1 Sensuicho, Tobata, Kitakyushu 804-8550, Japan

[b] JST, PRESTO, 4-1-8 Honcho Kawaguchi, Saitama 332-0012, Japan

[c] JST, ACT-C, 4-1-8 Honcho Kawaguchi, Saitama 332-0012, Japan

* Corresponding author. Tel.: +81 93 884 3318; fax: +81 93 884 3318.

E-mail address: tohno@che.kyutech.ac.jp (T. Ohno).

Abstract

Photocatalytic reduction of carbon dioxide (CO_2) was carried out using exposed-crystal-face-controlled titanium(IV) oxide (TiO_2) having a brookite phase. Methanol (CH_3OH) was detected as the main product, and trace amounts of formic acid, carbon monoxide, methane, and hydrogen were also detected in some cases. The prepared nanorod-shaped brookite TiO_2 with large {210} and small {212} exposed crystal faces showed larger CH_3OH generation than that of commercial brookite TiO_2 powder (Kojundo Chemical Laboratory Co., Ltd.). The activity of a brookite TiO_2 nanorod for CO_2 reduction depended on its aspect ratio because the {210} crystal faced worked as a reduction site, whereas an oxidation site was assigned to {212} crystal faces. Photodeposition of gold (Au) or silver (Ag) nanoparticles on the nanorod-shaped brookite TiO_2 induced a dramatic increase in CH_3OH production because the deposited metal particles work as reductive sites for multi-electron reduction of CO_2. Among the co-catalyst-loaded brookite TiO_2 nanorods, nanorod-shaped brookite TiO_2 loaded with Ag showed higher activity. The source of carbon of CH_3OH obtained by CO_2 reduction is discussed on the basis of results of a labeling experiment using $^{13}CO_2$.

Keywords: Exposed-crystal-face-controlled TiO_2; Brookite TiO_2 nanorod; Separation of reaction sites; Reduction of carbon dioxide

1. Introduction

Practical application of photocatalysts in converting solar light to chemical energy has been an attractive research field [1-11]. Water splitting over photoirradiated semiconductor photocatalysts has become an important issue world wide [12-20] because hydrogen is a promising alternative fuel when fossil fuels become depleted. In addition, CO_2 reduction to produce usable products is an important topic from the viewpoint of not only an environmental issue but also artificial photosynthesis. Although reduction of CO_2 using semiconductors such as TiO_2 as a photocatalyst

was reported by Fujishima [21], progress in this field has been very slow compared to the progress made in development of water splitting for hydrogen evolution. Photocatalytic reaction using semiconductor photocatalysts has been reported to have the potential to reduce CO_2 into hydrocarbons using water as an electron donor. For example, oxide semiconductor photocatalysts including titanium(IV) oxide (TiO_2) can produce formic acid (HCOOH), formaldehyde (HCHO), methanol (CH_3OH), and methane (CH_4) [22-34]. However, quantum yields for photocatalytic CO_2 reduction have been low. One reason for the low yields is that most of the reactions for CO_2 reduction employ a multi-electron process with relatively high redox potential, as shown below. In addition, back reaction on the surface of a semiconductor photocatalyst easily proceeded, resulting in retardation of CO_2 reduction, because many kinds of intermediates would be involved in this multi-electron reaction.

$$CO_2 + 2H^+ + 2e^- \rightarrow HCOOH, (-0.57\ V\ vs\ NHE)$$

$$CO_2 + 2H^+ + 2e^- \rightarrow CO + H_2O, (-0.52\ V\ vs\ NHE)$$

$$CO_2 + 4H^+ + 4e^- \rightarrow HCHO, (-0.48\ V\ vs\ NHE)$$

$$CO_2 + 6H^+ + 6e^- \rightarrow CH_3OH + H_2O, (-0.38\ V\ vs\ NHE)$$

$$CO_2 + 8H^+ + 8e^- \rightarrow CH_4 + 2H_2O, (-0.24\ V\ vs\ NHE)$$

Therefore, control of reaction sites on the surfaces of photocatalysts is a promising strategy for improvement of CO_2 reduction. In order to control reaction sites on the surface of a TiO_2 photocatalyst, we developed technology for controlling exposed crystal faces of TiO_2 nanoparticles [35-43]. The exposed crystal surfaces worked as reduction sites and oxidation sites separately, resulting in improvement of photocatalytic activity for organic pollutant decomposition. These surface properties should be useful for improvement of a multi-electron reaction such as CO_2 reduction because back reactions on the surfaces of photocatalysts would be drastically retarded.

Kominami et al. prepared single-phase brookite TiO_2 powder for the first time by solvothermal synthesis in which oxobis(2,4-pentanedionato-*O,O'*)titanium was used as the TiO_2 precursor and sodium laurate was used as a reagent for controlling the crystal structure [44]. They subsequently investigated the photocatalytic activity of single-phase brookite TiO_2 [45, 46].

Recently, other groups have also reported single-phase brookite TiO_2 having several kinds of characteristic structures, e.g., nanorods and nanotubes [47-51]. Among the three kinds of crystal structure of TiO_2, brookite TiO_2 show the highest reduction ability from evaluation of conduction band potential [52]. These properties are advantageous for CO_2 reduction. Therefore, we developed exposed-crystal-face-controlled brookite TiO_2 for CO_2 reduction.

In addition, metal co-catalyst loading on semiconductor photocatalysts is frequently carried out to enhance quantum yield and selectivity from CO_2 reduction into these products because appropriate co-catalysts work as reduction sites and enhance multi-electron reduction as a result of capturing electrons on metal particles [53-59, 31, 32, 34].

As mentioned above, we developed shape-controlled TiO_2 with specific exposed crystal faces in order to improve photocatalytic efficiency [35-43]. Utilization of the shape-controlled TiO_2 enhanced photocatalytic activity for decomposition of an organic compound because spatial separation of redox sites was induced by different kinds of exposed crystal faces [35-43]. Moreover, this property has advantages in co-catalyst loading by a photodeposition method, and site-selective co-catalyst loading on reduction faces by the photodeposition technique, which possibly decreases the recombination rate in co-catalyst particles, enhances photocatalytic activity by retarding back reactions. Actually, metal particles on reduction faces were observed in the shape-controlled TiO_2 [35-43].

In the present study, we confirmed the advantage of photocatalytic CO_2 reduction by exposed-crystal-face-controlled brookite TiO_2. Moreover, the effect of co-catalyst loading on the exposed-crystal-face-controlled brookite TiO_2 on activity for photocatalytic reduction of CO_2 was examined. Labeling experiments using $^{13}CO_2$ were also carried out in order to elucidate the carbon source of CH_3OH as a main product for CO_2 reduction on exposed-crystal-face-controlled brookite TiO_2 with co-catalyst loading.

2. Experimental Section

2.1. Materials

A titanium precursor (titaniumethoxide) was purchased from Sigma-Aldrich. Hydrogen peroxide (30%), ammonia, glycolic acid, polyvinyl alcohol (PVA), and polyvinyl pyrolidone (PVP) were purchased from Wako Pure Chemical Industries, Ltd. Glycolic acid was used to control the crystallinity and morphology of brookite TiO_2 particles. Commercial brookite TiO_2 powder was obtained from Kojundo Chemical Laboratory Co., Ltd. Other chemical reagents used in the present study were commercial products without further treatment.

2.2. Procedure for preparation of brookite TiO_2 nanorods without a polymer

Morphology-controlled brookite TiO_2 with {210} and {212} exposed crystal faces was prepared by hydrothermal synthesis [52, 60-62].

The procedure for preparation of morphology-controlled TiO_2 without an aspect ratio control reagent such as PVA is as follows. Milli-Q water (3.0 cm^3) was added to 10 cm^3 of titanium(IV) ethoxide and 50 cm^3 of ethanol with vigorous stirring, and the mixture was stirred for 30 min at room temperature. The resulting precipitate was centrifugally separated from the solution and dried under reduced pressure. The obtained amorphous titanium hydroxide particles (12.5 mmol) were dispersed in 30% hydrogen peroxide (40.0 cm^3). Then 25% ammonia (10.0 cm^3) and glycolic acid (18.75 mmol) were added, and yellow peroxo titanic acid (PTA) solution was obtained. After stirring the solution at ca. 60 °C for 6 h to remove excess amounts of hydrogen peroxide and ammonia, an orange gelled compound was obtained. The gelled compound was dispersed in Milli-Q water (3.0 cm^3) and pH of the solution was adjusted to 10 by addition of ammonia. Then the volume of the solution was adjusted (50.0 cm^3) by addition of Milli-Q water, and the solution in a Teflon bottle sealed with a stainless jacket (Sanaikagaku Co., HU-100) was heated at 200 ^oC for 48 h in an oven. After hydrothermal treatment, the residue in the Teflon bottle was washed with Milli-Q water until ionic conductivity of the supernatant was <10 $\mu S\ cm^{-1}$. The particles were dried under reduced pressure at 60 ^oC for 12 h.

2.3. Procedure for preparation of brookite TiO_2 nanorods with a polymer as an aspect ratio control reagent

Milli-Q water (3.0 cm^3) was added to 10 cm^3 of titanium(IV) ethoxide and 50 cm^3 of ethanol with vigorous stirring, and the mixture was stirred for 30 min at room temperature. The resulting precipitate was centrifugally separated from the solution and dried under reduced pressure. The obtained amorphous titanium hydroxide particles (25.0 mmol) were dispersed in 30% hydrogen peroxide (40.0 cm^3). Then 25% ammonia (10.0 cm^3) and glycolic acid (50.0 mmol) were added, and yellow peroxo titanic acid (PTA) solution was obtained. An aqueous solution containing an appropriate amount of PVA or PVP was added the PTA solution. After stirring the solution at room temperature for 6 h to remove excess amounts of hydrogen peroxide and ammonia, an orange gelled compound was obtained. The gelled compound was dispersed in Milli-Q water (3.0 cm^3) and pH of the solution was adjusted to 10 by addition of ammonia. Then the volume of the solution was adjusted (50.0 cm^3) by addition of Milli-Q water, and the solution in a Teflon bottle sealed with a stainless jacket (Sanaikagaku Co., HU-100) was heated at 200 ^oC for 48 h in an oven. After hydrothermal treatment, the residue in the Teflon bottle was washed with Milli-Q water until ionic conductivity of the supernatant was <10 μS cm^{-1}. The particles were dried under reduced pressure at 60 ^oC for 12 h.

2.4. Photodeposition of Au or Ag co-catalyst on brookite TiO_2 particles

For photodeposition of Au, an aqueous suspension consisting of brookite TiO_2 particles (200 mg) and 50 mL of an ethanol solution (8 vol %) containing an appropriate amount of hydrogen tetrachloroaurate(III) tetrahydrate was photoirradiated with a light-emitting diode (Nichia, NCCU033), which emitted light at a wavelength of ca. 365 nm and an intensity of 0.3 mW cm^{-2}, under a nitrogen atmosphere with vigorous magnetic stirring for 24 h. For photodeposition of Ag, an aqueous suspension consisting of TiO_2 particles (200 mg) and 50 mL of Milli-Q water containing an appropriate amount of silver nitrate was photoirradiated under the same conditions. After irradiation, photodeposited samples were obtained by washing with water several times and drying.

The net amount of Au or Ag on the TiO_2 surface was estimated by analysis of the filtrate with inductively coupled plasma optical emission spectroscopy (ICPOES; Shimadzu, ICPS-8000). ICP analysis revealed that the net molar amounts of Au and Ag compounds photodeposited on the brookite TiO_2 by photodeopsition were more than 99% of the provided molar amounts of Au and Ag.

2.5. Characterization of prepared samples

Crystal structures of the TiO_2 powders were characterized by using an X-ray diffractometer (Rigaku, MiniFlex II) with Cu Kα radiation (λ = 1.5405 Å). Primary particle sizes of the prepared samples were estimated from peaks at 37^o which are attributed to brookite {121} in XRD patterns using the Scherrer equation: $d = 0.9\lambda/\beta\cos\theta$, where λ is the wavelength of X-rays, θ is the Bragg angle and β is the full width at half maximum. β was estimated by fitting the XRD patterns with a superposition of Lorentz functions for peaks attributed to brookite. Diffuse reflectance (DR) spectra were measured using a UV-VIS spectrometer (Shimadzu, UV-2500PC and 2600) equipped with an integrating sphere unit (ISR-240A and ISR-2600plus). Specific surface area (S_{BET}) of the particles was determined with a surface area analyzer (Quantachrome, Nova 4200e) by using the Brunauer–Emmett–Teller equation. The morphology of prepared TiO_2 particles was observed by using a scanning electron microscope (SEM; JEOL, JSM-6701FONO) and a transmission electron microscope (TEM; Hitachi, H-9000NAR). X-ray photoelectron spectroscopy (XPS) spectra were obtained by using Kratos AXIS NOVA equipped with an Al Kα X-ray source of the dual anode. The shift of binding energy was corrected using the C 1s level at 284.6 eV as an internal standard. The net amounts of Au or Ag compounds on the hybrid photocatalysts were estimated by analysis of the filtrate with inductively coupled plasma optical emission spectroscopy (ICP-OES; Shimadzu, ICPS-8000).

2.6. Photocatalytic reduction of CO_2

Before evaluation of the photocatalytic activity, each sample was irradiated with UV light

using black light (UVP, XX-15BLB) in order to remove organic compounds on the sample. Photocatalytic reduction of CO_2 was carried out under ambient pressure. A light-emitting diode (Nichia, NCCU033), which emitted light at a wavelength of ca. 365 nm and an intensity of 0.3 mW cm^{-2}, was used as the light source for photocatalytic evaluation, and a test tube containing 5 mg of TiO_2 and 5 mL of 0.2 mol L^{-1} $KHCO_3$ aqueous solution saturated with CO_2 was photoirradiated with stirring for 24 h. Reaction products in liquid and gas phases were analyzed by gas chromatography (Hitachi G-3500, FID detector) with DB-WAXETR columns, gas chromatography (GL Science 490-GC, micro TCD detector) with MS-5A columns, and ion chromatography (Dionex, ICS-900) with IonPac AS-12A columns. Spherical shaped brookite TiO_2 was used as commercial brookite TiO_2 powder.

Apparent quantum efficiency (QE) was defined by the following equation because of a 6-hole process for production of CH_3OH as a main product from CO_2 reduction.

$$\mathrm{QE} = \frac{Number\ of\ reacted\ electrons}{Number\ of\ incident\ photons} \times 100$$

$$= \frac{Number\ \mathrm{of}\ generated\ CH_3OH\ molecules \times 6}{Number\ of\ incident\ photons} \times 100$$

2.7. Reactivity evaluation of exposed crystal faces by photodeposition of Pt and lead(IV) oxide (PbO_2) on brookite TiO_2 nanorods

Photodeposition of Pt and PbO_2 were carried out to determine reduction and oxidation sites on TiO_2 particles, respectively [63]. For determination of reduction sites, exposed crystal surface photodeposition of Pt was performed. An aqueous brookite TiO_2 nanorod suspension (2 g L^{-1}) containing 0.52 M 2-propanol and 1 mM hexachloroplatinic acid ($H_2PtCl_6 \cdot 6H_2O$) was irradiated with a 300 W mercury UV lamp (WACOM Model XDS-501S) for 24 h. N_2 gas was vigorously purged through the suspension prior to UV irradiation. The light intensity was about 1 mW cm^{-2}. After irradiation, the color of the powder changed from white to silver, and the suspension was centrifuged and washed with distilled water and then collected as powder after drying for 5 h at 60

^{o}C under reduced pressure.

PbO_2 nanoparticles were deposited as a result of Pb^{2+} ion oxidation in order to identify oxidation sites on the surface of brookite TiO_2 nanorods. This reaction was carried out in an aqueous brookite TiO_2 nanorod suspension (2 g L^{-1}) containing 0.1 M $Pb(NO_3)_2$ under an aerated condition. The pH of the solution for this reaction was adjusted to 1.0 by the addition of nitric acid according to the literature [63]. After photoreaction for 24 h using a 500 W Hg lamp (USHIO Co. Ltd., SX-UI501HQ), the color of the powder changed from white to brown, indicating that PbO_2 had been deposited on the surface. The light intensity was about 0.1 W cm^{-2}. Pt and PbO_2 particles deposited on TiO_2 were observed in SEM, EDX and TEM images.

3. Results and Discussion

3.1. Characterization

Figure 1 shows an XRD pattern of the prepared TiO_2. The structure of prepared sample was attributed to single-phase brookite TiO_2. Figure 2 shows a TEM image of the prepared TiO_2. Rod-like morphology with a length of 115 nm and width of 35 nm, which were agreed with the primary particle size estimated from the XRD pattern. Assignment of these exposed crystal faces was confirmed by SEM (Fig. 3), TEM (Fig. 2) and selected area electron diffraction (SAED) analyses. The prepared TiO_2 showed a nanorod shape with large {212} and small {210} exposed crystal faces, indicating that the nanorod-shaped particles were single crystals. S_{BET} of the prepared TiO_2 was 45 m^2 g^{-1}.

3.2. Effect of PVA or PVP as an aspect ratio control reagent (T = 48 h, pH 7)

To determine the role of PVA or PVP in the reaction, we conducted a series of syntheses by varying the concentration of PVA or PVP. TEM and SEM images showed that addition of the PVA or PVP polymer resulted in control of the shape of TiO_2 nanorods. Figure 2 (a - b) shows TEM images of brookite TiO_2 nanorods obtained after hydrothermal treatment with different PVA

or PVP concentrations. TEM images without a polymer (Figure 2c) showed a rod-like shape with an aspect ratio of **2.7** and single crystalline quality of the brookite TiO_2 nanorod.

The aspect ratio of brookite TiO_2 nanorods was decreased by addition of PVA or PVP. The effect of aspect ratio control for a brookite TiO_2 nanorod by addition of PVA was greater than that by addition of PVP as shown in Fig. 2 (a – b). These results indicate that addition of 50 mg of PVA was sufficient to prepare brookite TiO_2 particles with a small aspect ratio (Figure S1). The aspect ratio of a brookite TiO_2 nanorod with specific exposed crystal faces is sensitive to photocatalytic activity for CO_2 reduction, as discussed in a later section. The ratio of exposed reduction sites to oxidation sites on the surface of a brookite TiO_2 nanorod should be controlled in order to improve CO_2 reduction. Under the optimized conditions, reduction sites on the surface of a brookite TiO_2 nanorod should be predominantly exposed.

3.3. Photodeposition of Pt and PbO_2 for determination of reduction and oxidation sites

In order to determine reactivity such as oxidation or reduction on the exposed crystal surface of brookite TiO_2, photodeposition of Pt and PbO_2 was carried out. The colors of TiO_2 powder after UV irradiation in the presence of H_2PtCl_6 and $Pb(NO_3)_2$ aqueous solutions changed to gray and brown, respectively **[63]**. These color change in brookite TiO_2 suggested that Pt and PbO_2 were deposited on the TiO_2 surface. Furthermore, the presence of Pt and Pb elements was confirmed by XPS analysis. Pt particles were efficiently deposited on the exposed crystal surface assigned to reduction site because of Pt^{4+} reduction. The oxidation site of exposed crystal surface was assigned to PbO_2 deposition because Pb^{4+} was oxidized to produce PbO_2 nanoparticles. Figure 4 shows TEM images of Pt- and PbO_2-deposited brookite TiO_2 nanorods that were prepared by 48 h of hydrothermal treatment with PTA solution containing glycolic acid without a polymer. Small particles were observed on the specific exposed face of the brookite TiO_2 nanorod. Small particles were assigned by TEM with EDX analysis to Pt or PbO_2 deposited on the reductive or oxidative crystal surface of the brookite TiO_2 nanorod (Fig. 4). Pt nanoparticles of ca. 10 nm in size were mainly observed on the {210} face of a brookite TiO_2 nanorod, while large PbO_2 particles

with sizes of more than 100 nm were deposited on the {212} face of a brookite TiO_2 nanorod. These smaller particles were not observed on TiO_2 particles before the photodeposition procedure (Fig. 4).

As described in a later section, a correlation was found between photocatalytic activity and surface structure of TiO_2 particles, and photocatalytic activity increased with increase in the aspect ratio of brookite TiO_2 nanorods, which indicate the ratio of {210} to {212} exposed crystal faces. This result suggests that brookite TiO_2 nanorods with a small surface area of {212} and large surface area of {210} are suitable for photocatalytic CO_2 reduction. The highest photocatalytic activity of a brookite TiO_2 nanorod prepared by 48 h of hydrothermal treatment in the absence of a polymer was mainly due to the larger surface areas of reduction sites on the nanorod TiO_2 structure with the largest aspect ratio.

3.4. Photocatalytic activity for CO_2 reduction over a brookite TiO_2 nanorod with exposed crystal surfaces

In this study, amounts of the gas phase products are a trace (under the detection limit of Gas chromatography) over photoirradiation of co-catalyst loaded brookite TiO_2. When bare brookite TiO_2 was used, amounts of H_2, CO, CH_4 products are about 8, 3, 0 nmol, respectively. And amount of HCOOH is 35 nmol under ionic chromatography. Eventually, CH_3OH is a main product for the CO_2 reduction by using prepared brookite TiO_2 photocatalysts without co-catalyst. Photocatalytic reductions of CO_2 in our systems were performed in an aqueous suspension of prepared brookite TiO_2 at pH 7.3. Under the condition, the ionic forms of CO_2 in aqueous media shouldbe a mixture of HCO_3^-, H_2CO_3. Redox potentials of CO_3^{2-}, H_2CO_3 are +0.209, +0.044 V vs NHE for methanol formation from CO_2 reduction, respectively [64]. In addition, redox potentials of HCO_3^- might be placed between +0.209 and +0.044 V vs NHE. Figure 5 shows CH_3OH generation for the prepared brookite TiO_2 nanorod and commercial brookite TiO_2, which are non shape-controlled particles with S_{BET} of 27 m^2 g^{-1}. CH_3OH production by the prepared brookite TiO_2 nanorod was 2-times greater than that by spherical shaped commercial brookite TiO_2. This result indicated that a

shape-controlled brookite TiO_2 nanorod with exposed crystal phases has higher activity for CO_2 reduction than non shape-controlled commercial brookite TiO_2, presumably due to separation of oxidation and reduction sites. Moreover, larger {210} and smaller {212} exposed crystal faces may be an ideal surface structure for a multi-electron process for CO_2 reduction.

As described above, the aspect ratio of a brookite nanorod was decreased by addition of PVA or PVP as an aspect control reagent to the reaction solution during hydrothermal treatment. Aspect ratio dependence of the photocatalytic activity of a brookite TiO_2 nanorod with exposed crystal surfaces for CO_2 reduction was observed. The photocatalytic activity of a brookite TiO_2 nanorod for CO_2 reduction was decreased when the aspect ratio of the brookite TiO_2 nanorod became lower by using PVA or PVP as an aspect ratio control reagent. Enlargement of {210} assigned to reduction sites is an important strategy for improvement of photocatalytic CO_2 reduction over a brookite TiO_2 nanorod under UV light.

3.5. Effect of co-catalyst loading on photocatalytic activity

For further improvement of photocatalytic activity for CO_2 reduction, Au or Ag particles as co-catalysts were loaded on the prepared brookite TiO_2 nanorod by the photodeposition method. It was expected that the co-catalysts would be deposited on {210} exposed crystal faces of the prepared brookite TiO_2 nanorod because reduction reaction ($Au^{3+} + 3e^- \rightarrow Au^0$, $Ag^+ + e^- \rightarrow Ag^0$) predominantly proceeds over {210} faces of a brookite TiO_2 nanorod. Actually, loaded co-catalyst particles were observed mainly on {210} exposed crystal faces of the samples with larger amounts of Au and Ag loading as shown in Fig. 6.

After photodeposition, the color of the samples changed depending on the kind of loading material and loading amount. The colors of Au-loaded and Ag-loaded samples immediately after photodeposition were dark purple and pale henna, respectively. The colors of the samples correspond to localized surface plasmon resonance (LSPR) absorption of Au and Ag [65-68], and this implies that some of the Au and Ag particles were present as a metal state. However, the color of Ag-loaded samples changed after pre-treatment for photocatalytic activity (UV irradiation for

removal of organic compounds on the sample), indicating that aggregation of Ag nanoparticles or oxidation of Ag to generate Ag_2O might have occurred [34]. Figure 7 shows DR spectra of the prepared brookite TiO_2 nanorod with Au or Ag loading just before photocatalytic evaluation. Absorption peaks around 550 nm and 500 nm, which correspond to LSPR of Au and Ag on TiO_2, were observed in Au-loaded and Ag-loaded TiO_2 samples, respectively [65-67]. This implies that some of the Au and Ag particles were presumably present as a metal state after the pre-treatment for photocatalytic activity. Actually, XPS measurements were carried out on the Au-loaded and Ag-loaded TiO_2 samples (Figure S2). XPS spectra showed that loaded Ag particles were present as a mixture of Ag and Ag_2O. In contrast, the XPS spectrum confirmed that loaded Au particles were present as metal without other oxidation states. This coincides with the unchanged color of Au-loaded samples after the pre-treatment for photocatalytic activity.

Figure 8 shows CH_3OH generation of the prepared brookite TiO_2 nanorod with Au or Ag loading. CH_3OH generation showed an optimum amount with co-catalyst loading in all cases. In photocatalytic reaction systems, CO_2 reduction usually competes with H_2 evolution as a result of H^+ reduction. For instance, H_2 evolution predominantly occurs over Pt-loaded TiO_2 particles. On the other hand, Ag loading on the surface of a brookite TiO_2 nanorod induces predominant CO_2 reduction. Therefore, loading an optimum amount of a co-catalyst on the surface of brookite TiO_2 improves the selectivity between CO_2 reduction and H_2 evolution as well as the photocatalytic activity for CO_2 reduction. Although the key mechanism for highly selective CO_2 reduction on co-catalyst-loaded brookite TiO_2 is under investigation, preferential CO_2 adsorption on a co-catalyst loaded on the surface of TiO_2 particles might be one of the key steps for improving predominant CO_2 reduction.

Increase in CH_3OH generation on brookite TiO_2 loaded with a co-catalyst was presumably due to prevention of recombination and/or enhancement of selectivity for CH_3OH generation as a result of multi-electron reduction by electron capturing on metal particles. This effect was probably influenced by properties of co-catalyst particles, e.g., loading site, amount, particle size and dispersibility. Decrease in CH_3OH generation with an excess amount of the co-catalyst may

be due to the filter effect caused by photoabsorption and/or light scattering of co-catalyst particles. Actually, relative reflectance of the samples in the wavelength of more than 400 nm increased with an increase in loading amount (Fig. 8). Moreover, excess amount of co-catalyst loading may result in covering active sites or absorption sites of reactants and loss of appropriate properties as co-catalyst particles, such as dispersibility and particle size.

In order to elucidate the influence of particle size on CH_3OH generation, absorption peaks attributed to LSPR of Au and Ag particles were evaluated in UV-VIS spectra (Fig. 8). Figure 8 shows absorption wavelength of the peak (λ_p) attributed to LSPR of Au and Ag as a function of amount of co-catalyst loading. A red shift of LSPR peak was usually observed by particle size growing and aggregation state of metal particles [68-70].

The peaks of Au-loaded samples showed dependence on loading amount up to 0.1 wt%. This indicates that the decrease in CH_3OH generation by the 0.1 wt% Au-loaded sample was mainly caused by an increase in particle size and decrease in dispersion of Au particles. In contrast, the peaks of Ag-loaded samples were only slightly red-shifted with an increase in loading amount. This indicates that decrease in CH_3OH generation with a larger amount of Ag loading might be due to the filter effect.

Therefore, CH_3OH generation of the Au-loaded brookite TiO_2 nanorod was influenced by particle size and/or aggregation state in addition to the effect observed in the Ag-loaded sample.

3.6. Labeling experiments using $^{13}CO_2$ reduction of CO_2

We applied ^{1}H-NMR spectroscopy for analyzing the carbon source of CH_3OH. Labeling experiment by using $^{13}CO_2$ for CO_2 reduction was taken place over Au loaded brookite TiO_2 nanorod for 24 h under UV light irradiation. Before evaluation of the photocatalytic activity, each sample was irradiated with UV light using black light (UVP, XX-15BLB) for 1 day in order to remove organic compounds on the sample. Degas and purge $^{13}CO_2$ processes were shown in Fig. 9. Photocatalysts powder 5 mg were ultrasonically dispersed in deionized water (5 mL). After complete degassing the whole system by diaphragm pump (Process 1), $^{13}CO_2$ gas was bubbling for

15 min (Process 2). CO_2 photoreduction is performed for 24 h during UV irradiation (Process 3). After the reaction, the photocatalysts was removed by centrifugal separation. The aqueous samples (4 ml) for ^{1}H-NMR are dissolved in D_2O (1 ml). 3-(Trimethylsilyl)-1-propanesulfonic acid sodium salt (SIGMA-ALDRICH) was used as an internal standard compound. In the ^{1}H-NMR of the same solution, a doublet (J_{CH} = 142 Hz) attributable to the proton coupled to the ^{13}C of $^{13}CH_3O-$ was observed at 3.34 ppm, but no singlet due to the proton of $^{12}CH_3O-$ was detected (Figure 10). These results clearly show that the carbon source of CH_3OH is $^{13}CO_2$.

4. Conclusion

Brookite TiO_2 particles with specific exposed crystal faces were prepared by hydrothermal treatment. In addition, PVP or PVA was used as an aspect control reagent. The aspect ratio of the prepared brookite TiO_2 nanorod was controlled by addition of PVA or PVP.

Photocatalytic CO_2 reduction using brookite TiO_2 nanorods with large {210} and small {212} exposed crystal faces were carried out. CH_3OH was obtained as the main product for CO_2 reduction over a brookite TiO_2 nanorod under UV light. Photocatalytic activity of a brookite TiO_2 nanorod for CO_2 reduction is higher than that of spherical-shaped commercial brookite TiO_2. In addition, a brookite TiO_2 nanorod with larger aspect ratio showed higher photocatalytic activity than that with a smaller aspect ratio. This indicates that larger {210} and smaller {212} exposed crystal faces prevented back reaction and enhanced multi-electron reduction as a result of separation of redox sites. Au or Ag loading on the reduction crystal surface of the prepared brookite TiO_2 nanorod increased CH_3OH generation. The mechanisms of activity enhancement by the loading of metals might be different. Au loading increased selectivity for CH_3OH generation to some extent. On the other hand, loading of Ag with appropriate properties resulted in a larger increase in CH_3OH generation than that in the case of Au, though Ag has no selectivity for CH_3OH generation. The carbon source of CH_3OH, which is the main product of CO_2 reduction over a brookite TiO_2 nanorod, was confirmed by a labeling experiment using $^{13}CO_2$.

Acknowledgements

This work was supported by the JST PRESTO program and the JST ACT-C program.

Figure Captions

Figure 1. XRD pattern

Figure 2. TEM images of brookite TiO_2 nanorod (a) with PVA (b) with PVP and (c) without polymer

Figure 3. SEM images of the prepared brookite TiO_2 nanorod (a) with PVA (b) with PVP and (c) without polymer

Figure 4. TEM images and EDX analyses of Pt or PbO_2 loaded brookite TiO_2 nanorods (a) Pt (b) PbO_2

Figure 5. Amount of CH_3OH generated over several kinds of brookite TiO_2 (commercial brookite TiO_2, the prepared brookite TiO_2 with PVA, PVP and without polymer

Figure 6. TEM images of brookite TiO_2 nanorods (a) bare sample and (b) Au loaded brookite TiO_2 and (c) Ag loaded brookite TiO_2

Figure 7. DR spectra of metal co-catalysts loaded brookite TiO_2 nanorods (a) Au and (b) Ag

Figure 8. Amount of CH_3OH generated over the metal co-catalysts loaded brookite TiO_2 nanorods as a function of amount of co-catalysts (a) Au (b) Ag

Figure 9. Process of experiments reduction of CO_2 using $^{13}CO_2$.

Figure 10. ^{1}H-NMR spectra of Au-loaded brookite TiO_2 nanorod

Figure S1. SEM images of the change in particle size of TiO_2 with different amounts of PVA added.

Figure S2. XPS spectra of the metal co-catalysts loaded brookite TiO_2 nanorods (a) Au (b) Ag

References

[1] A. Fujishima, K. Honda, Nature. 238(1972) 37–38.

[2] A. Fujishima, T. N. Rao, D. A. Tryk, J. Photochem. Photobiol. C. 1 (2000) 1–21.

[3] Y. Shiraishi, T. Hirai, J. Photochem. Photobiol. C. 9 (2008) 157–170.

[4] B. Ohtani, J. Photochem. Photobiol. C. 11 (2010) 157–178.

[5] T. Yui, Y. Kobayashi, Y. Yamada, K. Yano, Y. Fukushima, T. Torimoto, K. Takagi, ACS Appl. Mater. Interfaces. 3 (2011) 931–935.

[6] T. Yui, T. Tsuchino, H. Mino, T. Kajino, S. Itoh, Y. Fukushima, K. Takagi, Bull. Chem. Soc. Jpn. 82 (2009) 914–916.

[7] T. Yui, Y. Kobayashi, Y. Yamada, T. Tsuchino, K. Yano, T. Kajino, Y. Fukushima, T. Torimoto, H. Inoue, K. Takagi, Phys. Chem. Chem. Phys. 8 (2006) 4585–4590.

[8] T. Tachikawa., T. Yui., M. Fujitsuka, K. Takagi, T. Majima, Chem. Lett. 34 (2005) 1522–1523.

[9] P. G. Hoertz, T. E. Mallouk, Inorg. Chem. 44 (2005) 6828–6840.

[10] A. C. Benniston, A. Harriman, Mater. Today. 11 (2008) 26–34.

[11] T. E. Mallouk, J. Phys. Chem. Lett. 1 (2010) 2738–2739.

[12] R. Abe, J. Photochem. Photobiol. C. 11 (2010) 179–209.

[13] M. Higashi, R. Abe, T. Takata, K. Domen, Chem. Mater. 21 (2009) 1543–1549.

[14] K. Maeda, K. Teramura, D. Lu, T. Takata, N. Saito, Y. Inoue, K. Domen, Nature. 440 (2006) 295.

[15] I. Tsuji, Y. Shimodaira, H. Kato, H. Kobayashi, A. Kudo, Chem. Mater. 22 (2010) 1402–1409.

[16] Y. K. Kho, A. Iwase, W. Y. Teoh, L. Madler, A. Kudo, R. Amal. J. Phys. Chem. C. 114 (2010) 2821–2829.

[17] H. Kaga, K. Saito, A. Kudo, Chem. Commun. 46 (2010) 3779–3781.

[18] H. Kato, Y. Sasaki, A. Iwase, A. Kudo, Bull. Chem. Soc. Jpn. 80 (2007) 2457–2464.

[19] H. Kato, K. Asakura, A. Kudo, J. Am. Chem. Soc. 125 (2003) 3082–3089.

[20] W. J Youngblood, S. H. A. Lee, K. Maeda, T. E. Mallouk, Acc. Chem. Res. 42 (2009) 1966–1973.

[21] T. Inoue, A. Fujishima, S. Konishi, K. Honda, Nature. 277 (1979) 637-638.

[22] F. Solymosi, I. Tombácz, Catal. Lett. 27 (1994) 61-65.

[23] M. Anpo, H. Yamashita, Y. Ichihashi, Y. Fujii, M. Honda, J. Phys. Chem. B. 101 (1997) 2632-2636.

[24] I.. H. Tseng., J. C. S. Wu, H. Y. Chou, J. Catal. 221 (2004) 432-440.

[25] Q. H. Zhang, W. D. Han, Y. J. Hong, J. G. Yu, Catal. Today. 148 (2009) 335-340.

[26] K. Koci, K. Mateju, L. Obalova, S. Krejcikova, Z. Lancy, D. Placha, L. Capek, A. Hospodkova, Solcova, O. 96 (2010) 239-244.

[27] T. Yui, A. Kan, C. Saitoh., K. Koike., T. Ibusuki, O. Ishitani, ACS Appl. Mater. Interfaces. 3 (2011) 2594-2600.

[28] K. Sayama, H. Arakawa, J. Phys. Chem. 97 (1993) 531-533.

[29] Y. Matsumoto, M. Obata, J. Hombo, J. Phys. Chem. 98 (1994) 2950-2951.

[30] P. W. Pang, Y. W. Chen, Catal. Commun. 8 (2007) 1546-1549.

[31] Q. Liu, Y. Zhou, J. Kou, X. Chen, Z. Tian., J. Gao, S. Yang, Z. Zou, J. Am. Chem. Soc. 132 (2010) 14385-14387.

[32] S. C. Yan, S. X. Ouyang, J. Gao, M. Yang, J. Y. Feng, X. X. Fan, L. J. Wan, Z. S. Li, J. Ye, Y. Zhou, Z. G. Zou, Angew. Chem. Int. Ed. 49 (2010) 6400-6404.

[33] Y. Zhou, Z. Tian, Z. Zhao, Q. Liu, J. Kou, X. Chen, J. Gao, S. Yan, Z. Zou, ACS Appl. Mater. Interfaces. 3 (2011) 3594-3601.

[34] K. Iizuka, T. Wato, Y. Miseki, K. Saito, K. Kudo, J. Am. Chem. Soc. 133 (2011) 20863-20868.

[35] E. Bae, N. Murakami, T. Ohno, J. Mol. Catal. A: Chem. 300 (2009) 72-79.

[36] N. Murakami., Y. Kurihara, T. Tsubota, T. Ohno, J. Phys. Chem. C. 113 (2009) 3062-3069.

[37] E. Bae, N. Murakami, M. Nakamura, T. Ohno, Appl. Catal. A: Gen. 380 (2010) 48-54.

[38] L. Zhang, V. M. Menendez-Flores, N. Murakami, T. Ohno, Appl. Surf. Sci. 258 (2012) 5803-5809.

[39]N. Murakami, S. Kawakami, T. Tsubota, T. Ohno, J. Mol. Catal. A: Chem. 358 (2012) 106-111.

[40] V. M. Menendez-Flores, M. Nakamura, T. Kida, Z. Jin, N. Murakami, T. Ohno, Appl. Catal. A: General. 406 (2011) 119-123.

[41] N. Murakami, A. Ono, M. Nakamura, T. Tsubota, T. Ohno, Appl. Catal. B: Environ. 97 (2010)

115–119.

[42] E. Bae, T. Ohno, Appl. Catal. B, Environmental. 91 (2009) 634-639.

[43] N. Murakami, T. Kamai, T. Tsubota, T. Ohno, Cat. Commun. 10 (2009) 963-966.

[44] H. Kominami, M. Kohno, Y. Kera, J. Mater. Chem. 10 (2000) 1151.

[45] H. Kominami, J. Kato, S. Murakami, Y. Ishii, M. Kohno, K. Yabutani, T. Yamamoto, Y. Kera, M. Inoue, T. Inui, B. Ohtani, Cat. Today. 84 (2003) 181.

[46] H. Kominami, Y. Ishii, M. Kohno, S. Konishi, Y. Kera, B. Ohtani, Cat. Lett. 91 (2003) 41.

[47] A. Pottier, C. Chaneac, E. Tronc, L. Mazerolles, J.P. Jolivet, J. Mater. Chem. 11 (2001) 1116.

[48] K. Tomita, V. Petrykin, M. Kobayashi, M. Shiro, M. Yoshimura, M. Kakihana, Angew. Chem. Int. Ed. 45 (2006) 2378.

[49] M. Kakihana, K. Tomita, V. Petrykin, M. Yoshimura, M. Kakihana, J. Mater. Sci. 43 (2008) 2158.

[50] R. Buonsanti, V. Grillo, E. Carlino, C. Giannini, T. Kipp, R. Cingolani, P.D. Cozzoli, J. Am. Chem. Soc. 130 (2008) 11223.

[51] Q. Deng, M. Wei, X. Ding, L. Jiang, B. Ye, K. Wei, Chem. Comm. (2008) 3657.

[52] T. A. Kandiel, A. Feldhoff, L. Robben, R. Dillert, D. W. Bahnemann, Chem. Mat. 22 (2010) 2050-2060

[53] F. Solymosi, I. Tombácz, Catal. Lett. 27 (1994) 61-65.

[54] I. H. Tseng, J. C. S. Wu, H. Y. Chou, J. Catal. 221 (2004) 432-440.

[55] Q. H. Zhang, W. D. Han., Y. J. Hong, J. G. Yu, Catal. Today. 148 (2009) 335-340.

[56] K. Koci, K. Mateju, L. Obalova, S. Krejcikova, Z. Lancy, D. Placha, L. Capek, A. Hospodkova, O. Solcova, Appl. Catal. B: Environ. 96 (2010) 239-244.

[57] T. Yui, A. Kan, C. Saitoh, K. Koike, T. Ibusuki, O. Ishitani, ACS Appl. Mater. Interfaces. 3 (2011) 2594-2600.

[58] K. Sayama, H. Arakawa, J. Phys. Chem. 97 (1993) 531-533.

[59] P. W. Pang, Y. W. Chen, Catal. Commun. 8 (2007) 1546-1549.

[60] M. Kobayashi, K. Tomita, V. Petrykin, S. Yin, T. Sato, M. Yoshimura and M. Kakihana, Solid

State Phenomena. 124-126 (2007) 723-726.

[61] H. Zhang, J. F. Banfield, J. Phys. Chem. B. 104 (2000) 3481-3487.

[62] M. Kobayashi, V. Petrykin, M. Kakihana, K. Tomita, J. Am. Ceram. Soc. 92 [S1] (2009) S21–S26.

[63] T. Ohno, K. Sarukawa, M. Matsumura, New J. Chem. 26 (2002) 1167-1170.

[64] X. Yang, T. Xiao, P. P. Edwards, Int. J. Hydrog. Energy 36 (2011) 6546-6552.

[65] Y. Tian, T. Tatsuma, J. Am. Chem. Soc. 127 (2005) 7632-7637.

[66] K. Naoi, Y. Ohko, T. Tatsuma, J. Am. Chem. Soc. 126 (2004) 3664-3668.

[67] A. Zielinska, E. Kowalska, J. W. Sobczak, W. Liskowski, B. Ohtani, A. Zaleska, Appl. Catal. B Environ. 101 (2011) 504-514.

[68] S. Link., El. Sayed, M. A, J. Phys. Chem. B. 103 (1999) 4212-4217.

[69] R. Jin., Y. Cao, C. A. Mirkin, K. L. Kelly, G. C. Schatz, J. G. Zheng, Science. 294 (2001) 1901-1903.

[70] J. J. Mock., M. Barbic, D. R. Smith, D. A. Schultz, S. Schultz, J. Chem. Phys. 116 (2002) 6755-6759.

Fig.1

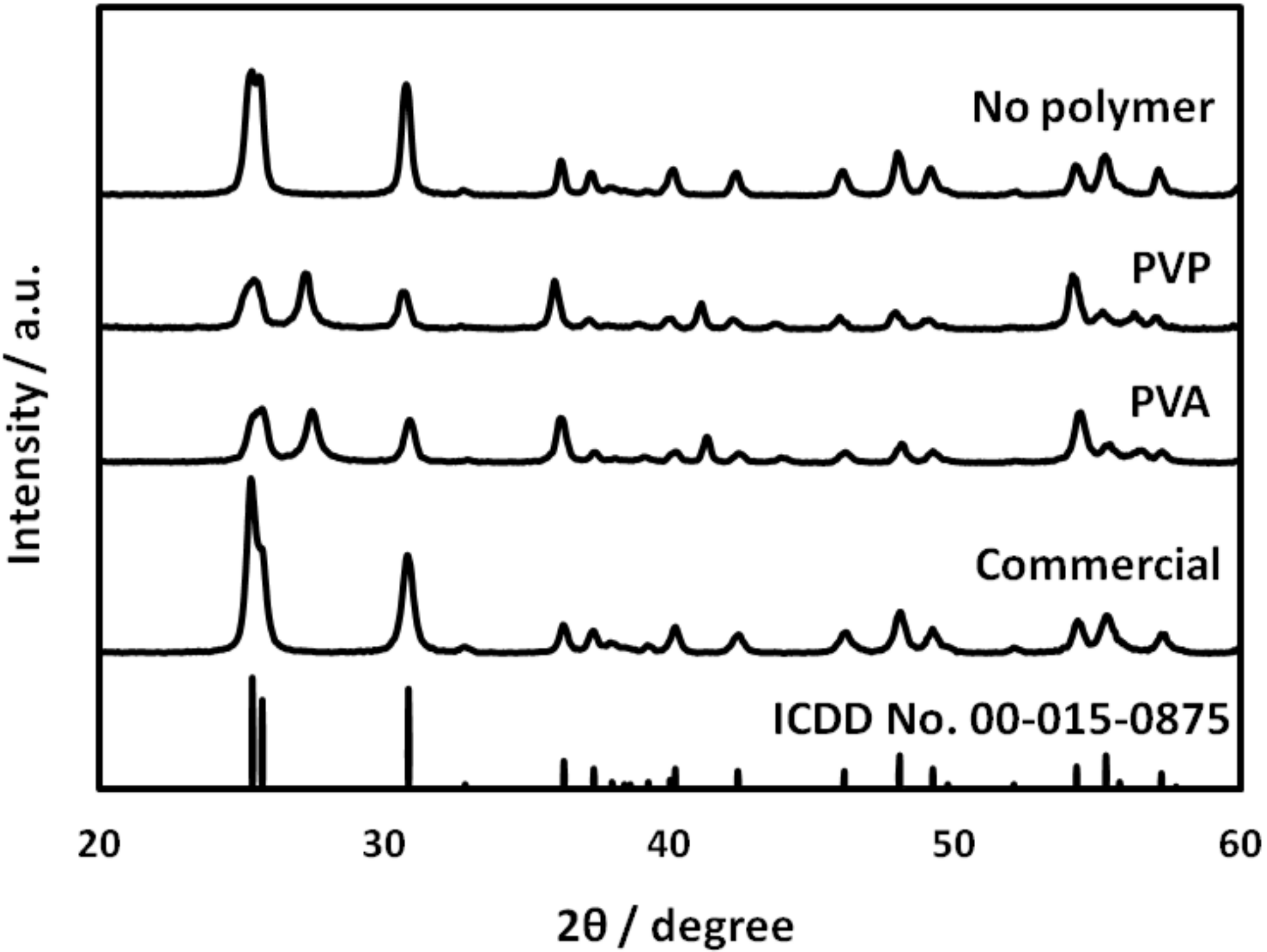
No polymer
PVP
PVA
Commercial
ICDD No. 00-015-0875
Intensity / a.u.
20
30
40
50
60
2θ / degree

Fig.2

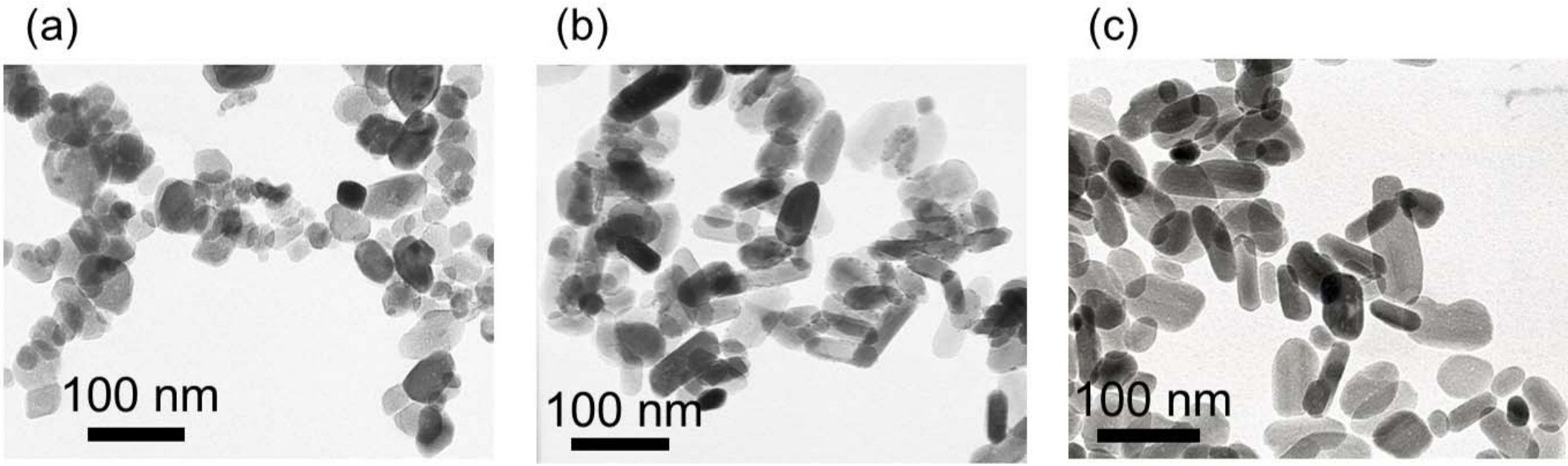

Fig.3

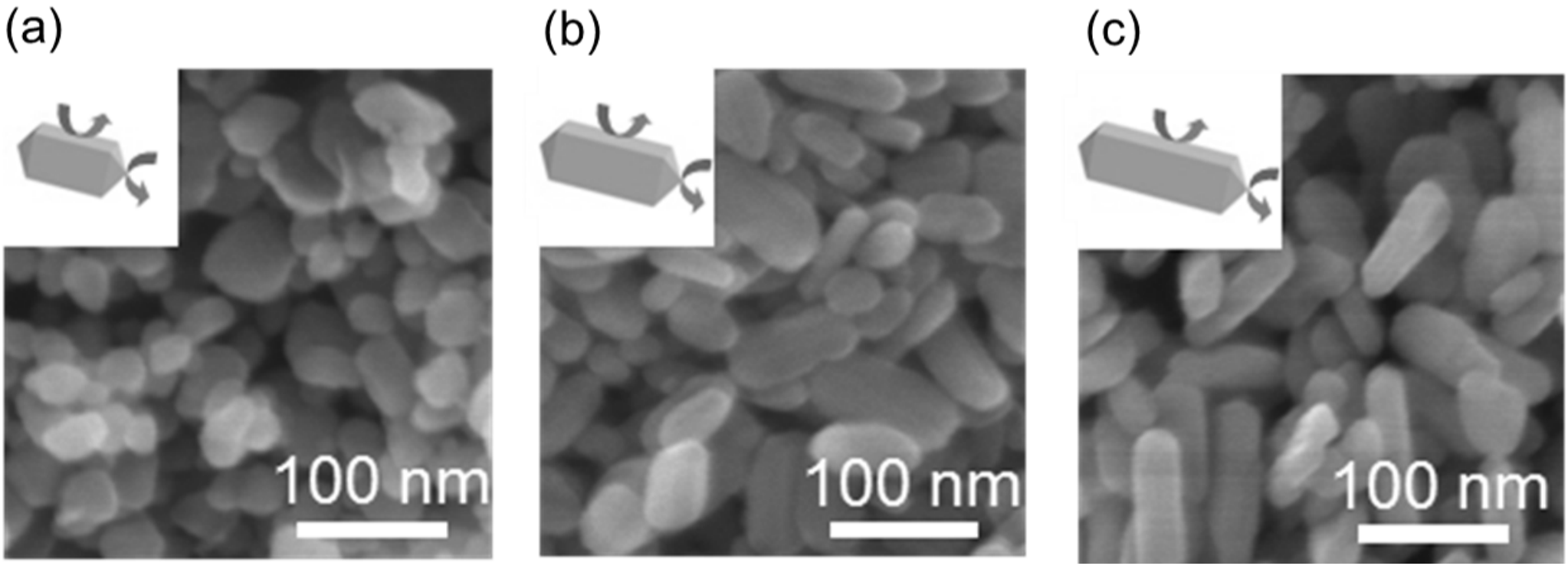

Fig.4

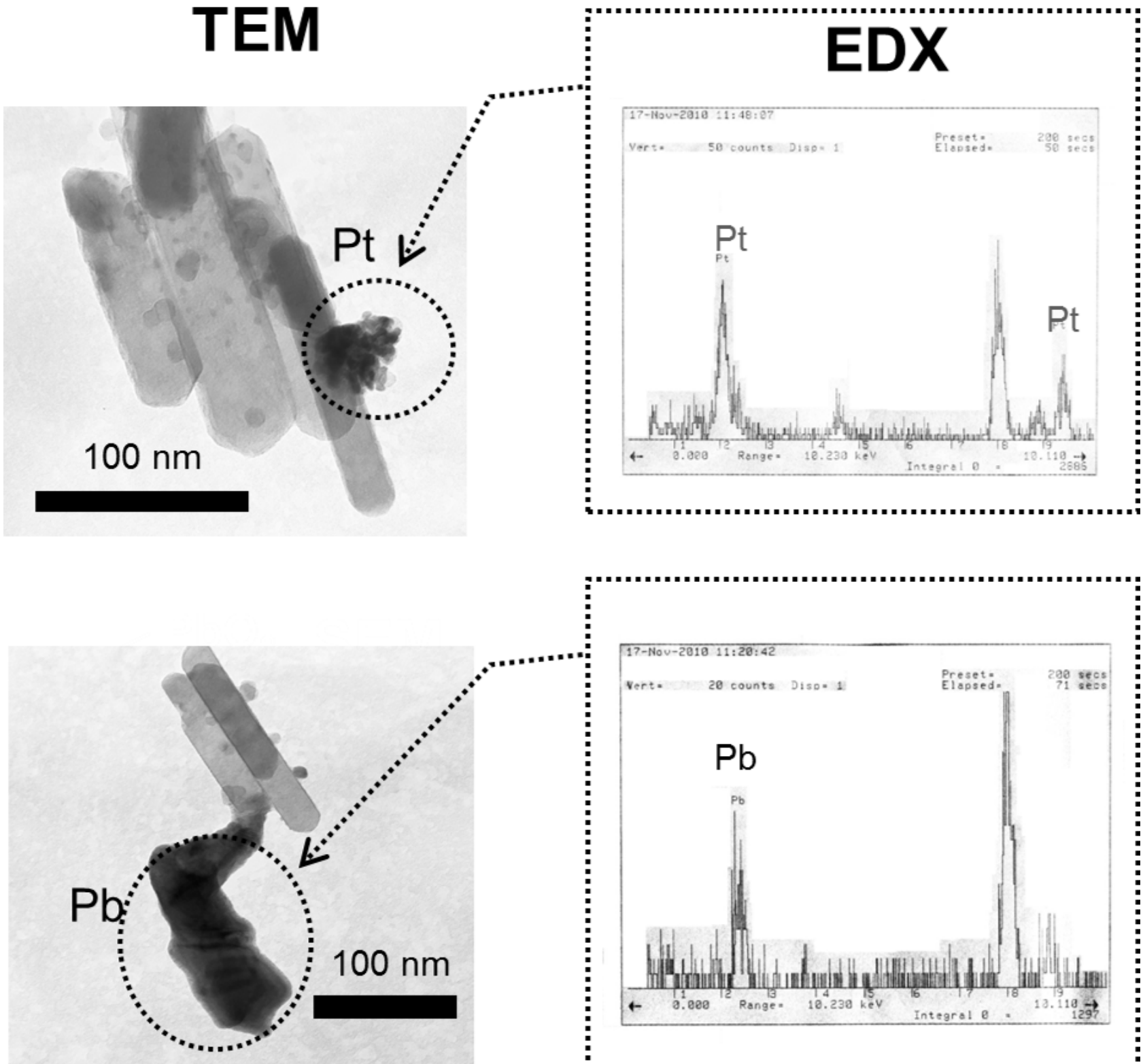
TEM
EDX
Pt
100 nm
17-Nov-2010 11:48:07
Vert= 50 counts Disp= 1
Preset= 200 secs
Elapsed= 50 secs
Pt
Pt
Pt
0.000 Range= 10.230 keV 10.110
Integral 0 = 2886
Pb
100 nm
17-Nov-2010 11:20:42
Vert= 20 counts Disp= 1
Preset= 200 secs
Elapsed= 71 secs
Pb
Pb
0.000 Range= 10.230 keV 13.110
Integral 0 = 1297

Fig.5

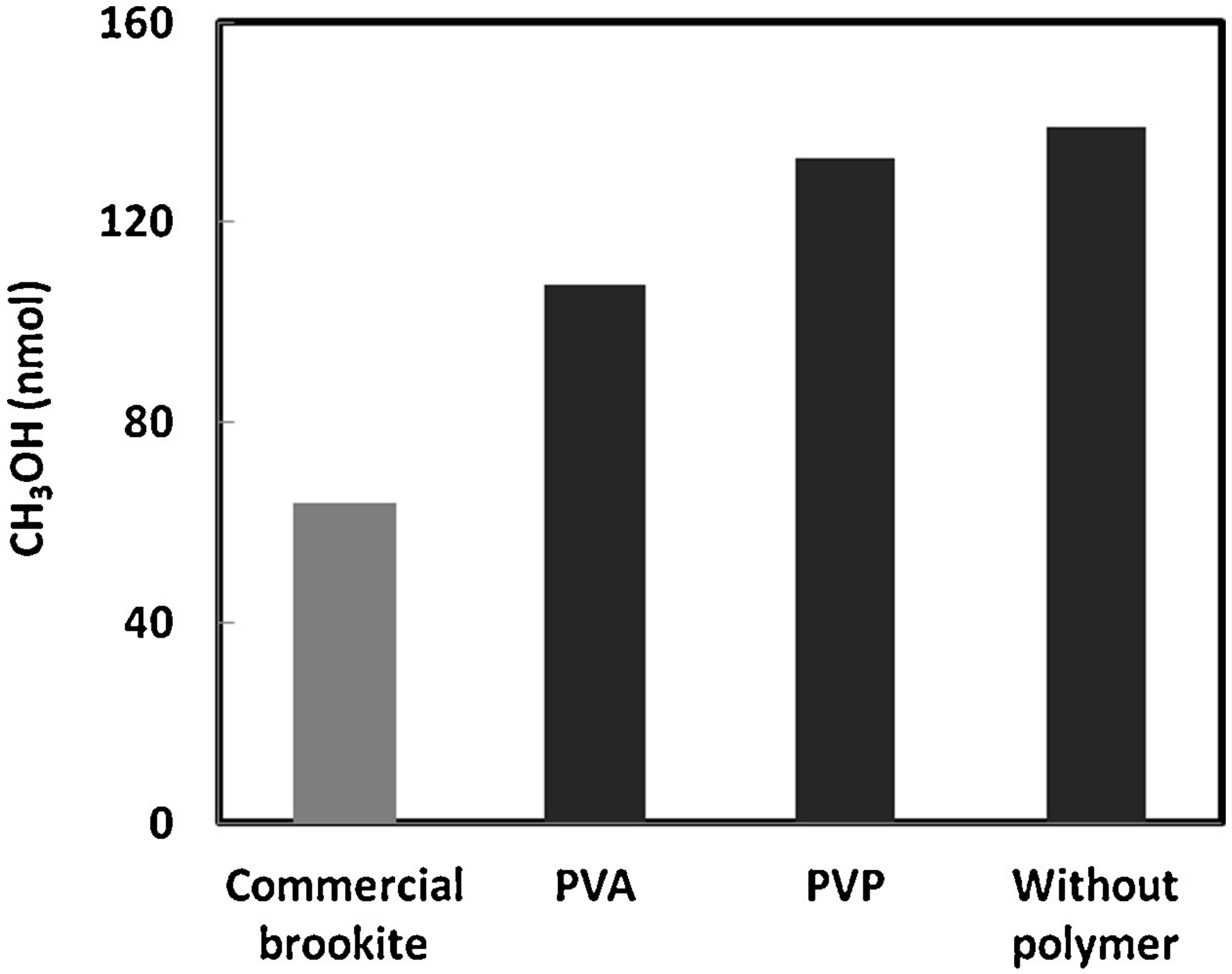
160
120
80
40
0
CH_3OH (nmol)
Commercial brookite
PVA
PVP
Without polymer

Fig.6

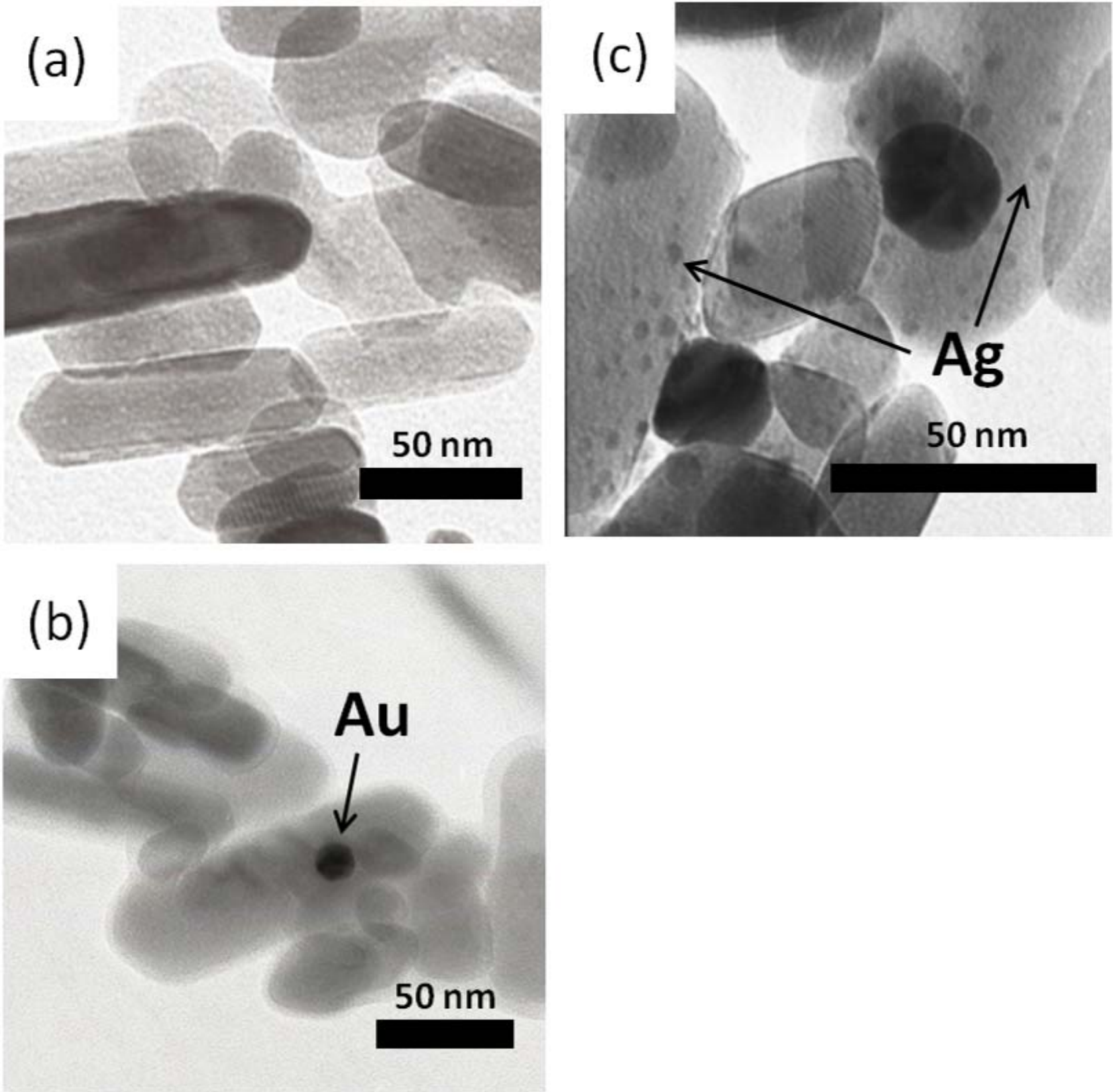

Fig.7(a)

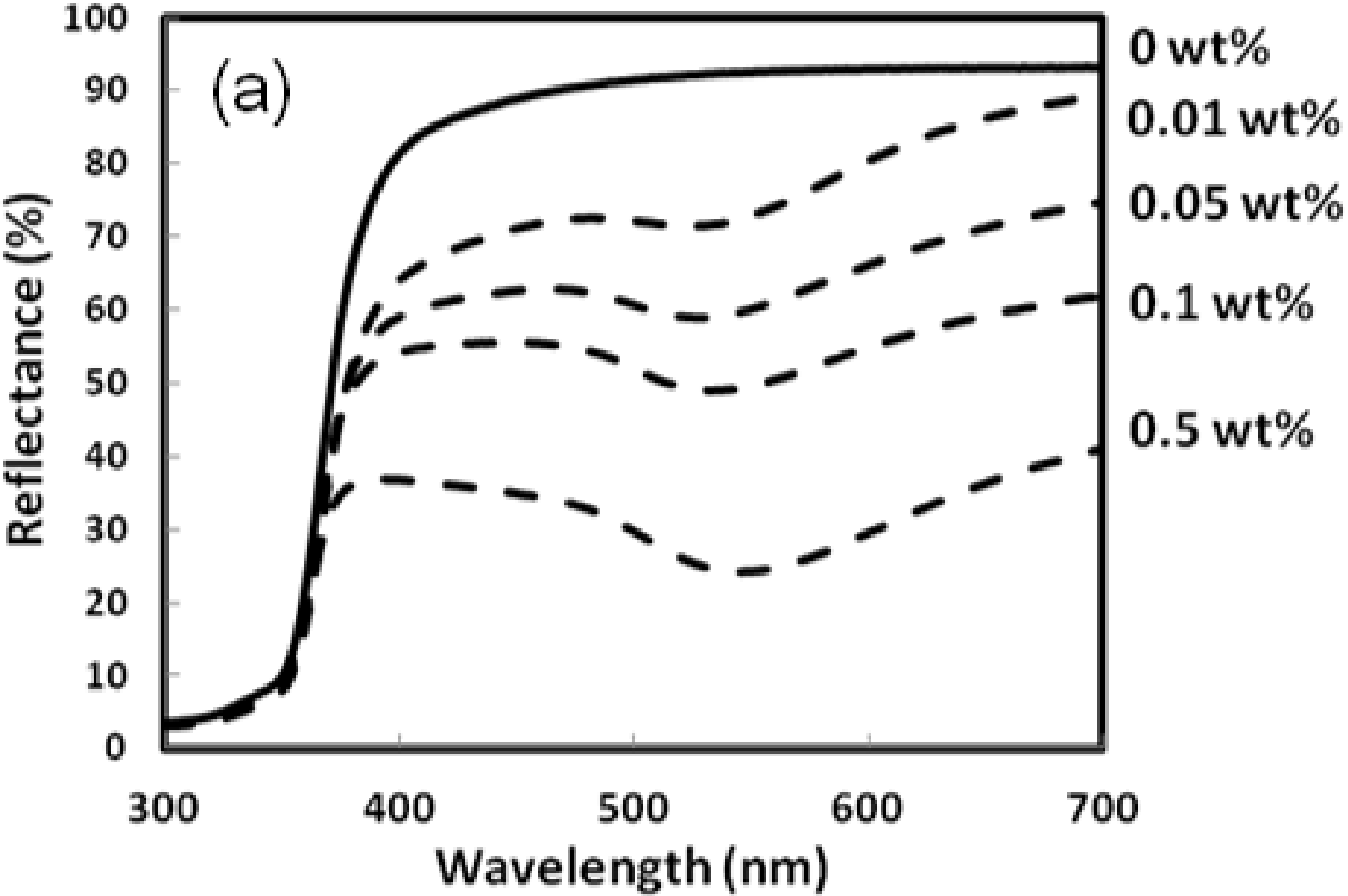
(a)
100
90
80
70
60
50
40
30
20
10
0
Reflectance (%)
300
400
500
600
700
Wavelength (nm)
0 wt%
0.01 wt%
0.05 wt%
0.1 wt%
0.5 wt%

Fig.7 (b)

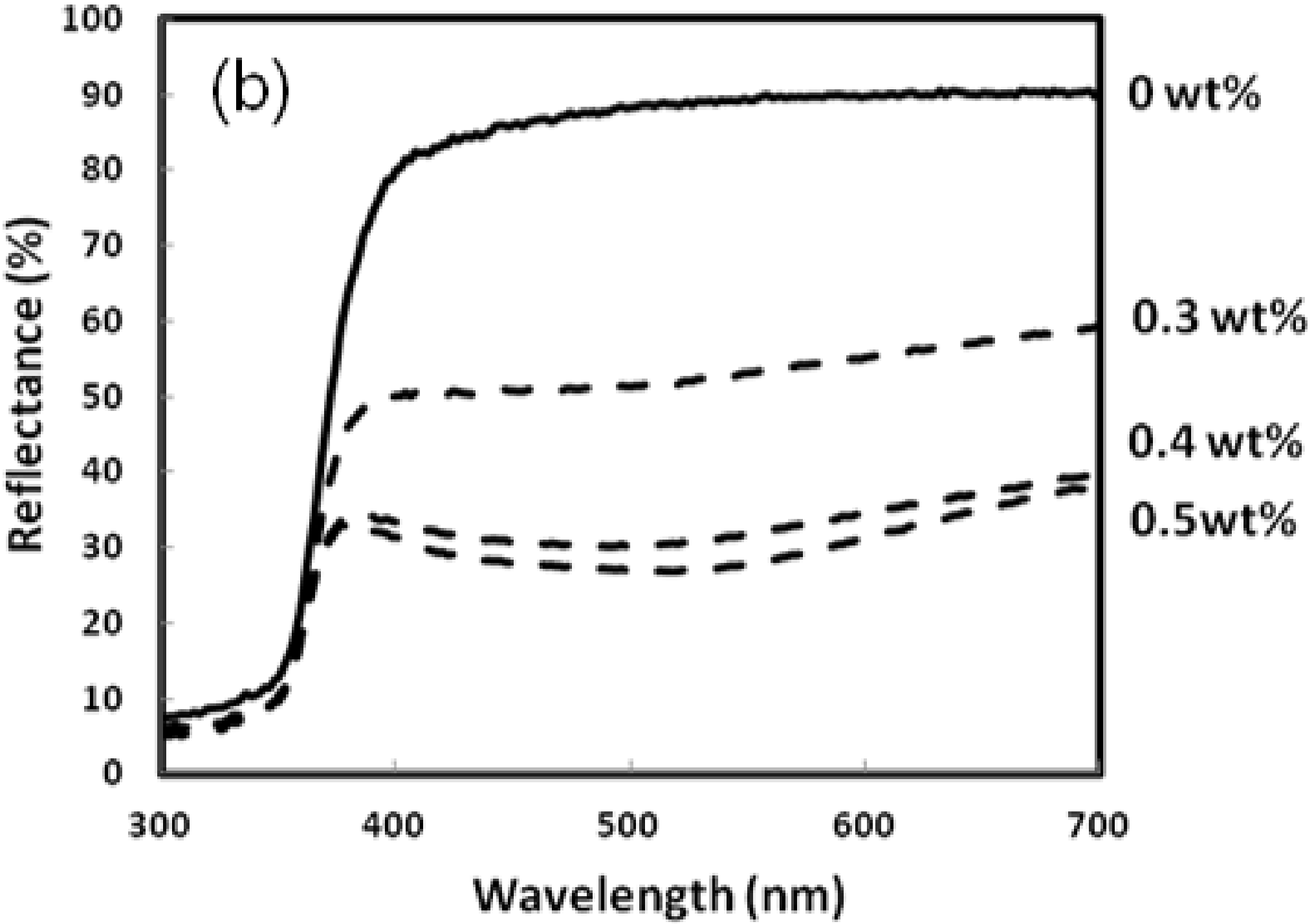
(b)
100
90
80
70
60
50
40
30
20
10
0
Reflectance (%)
300
400
500
600
700
Wavelength (nm)
0 wt%
0.3 wt%
0.4 wt%
0.5wt%

Fig.8(a)

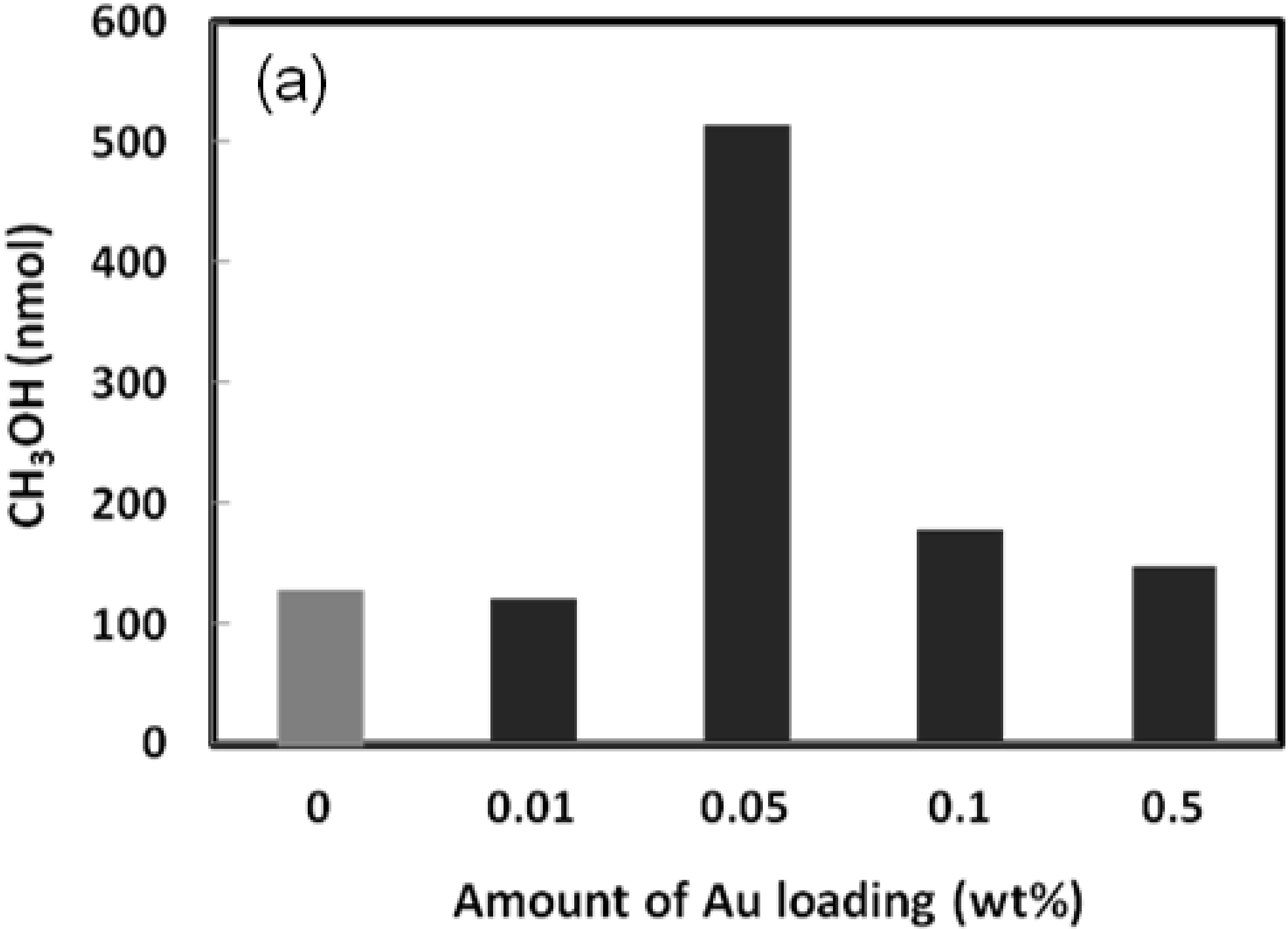
(a)
600
500
400
300
200
100
0
CH_3OH (nmol)
0
0.01
0.05
0.1
0.5
Amount of Au loading (wt%)

Fig.8(b)

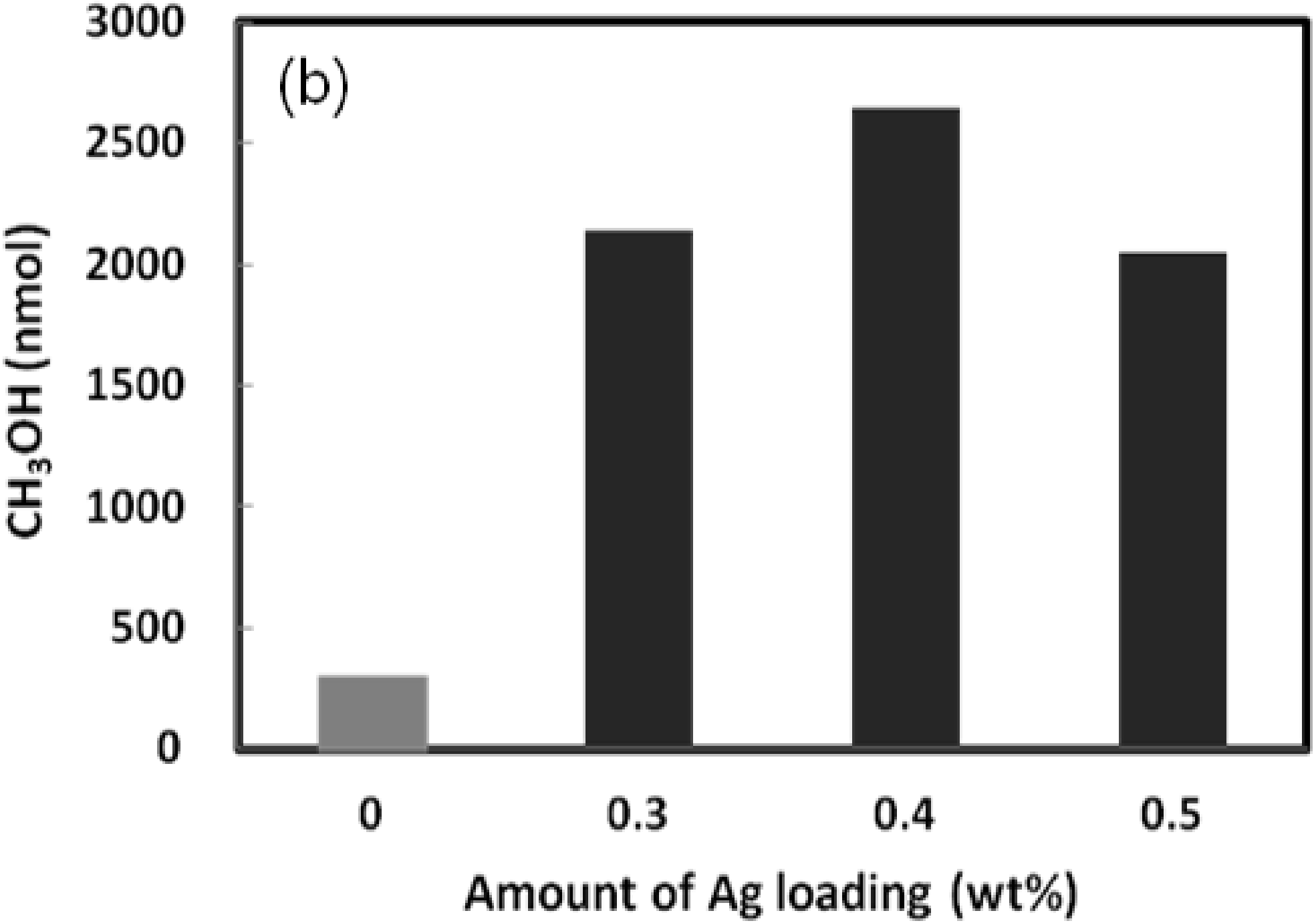
(b)
3000
2500
2000
1500
1000
500
0
CH_3OH (nmol)
0
0.3
0.4
0.5
Amount of Ag loading (wt%)

Fig.9

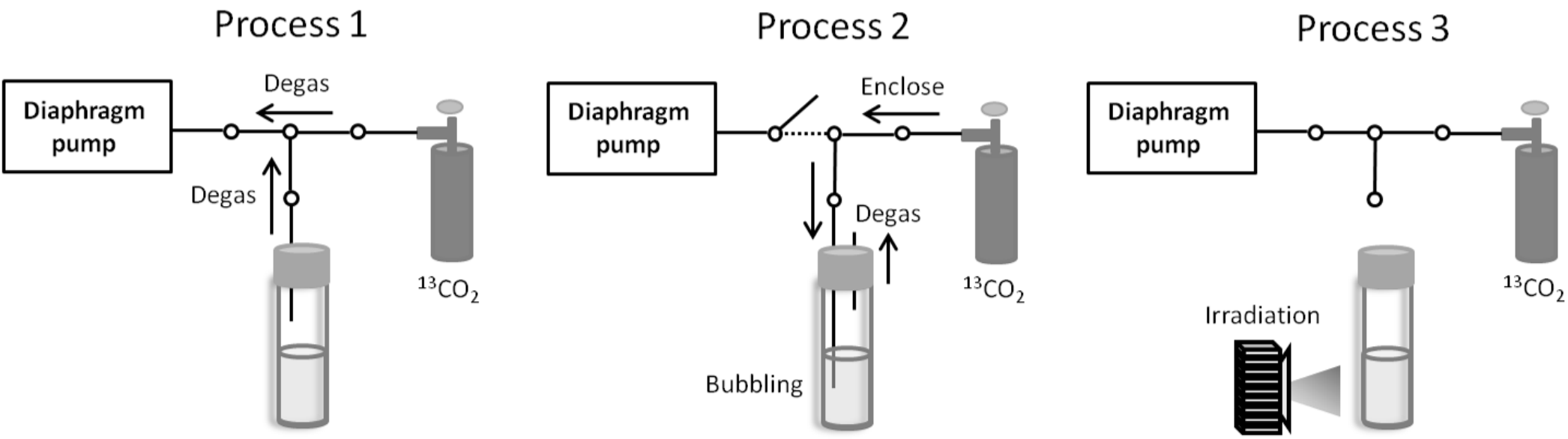
Process 1
Diaphragm pump
Degas
Degas
$^{13}CO_2$
Process 2
Diaphragm pump
Enclose
Degas
$^{13}CO_2$
Bubbling
Process 3
Diaphragm pump
$^{13}CO_2$
Irradiation

Fig.10